

# Preparation of poly(acrylic acid)/tricalcium phosphate nanoparticles scaffold: Characterization and releasing UC-MSCs derived exosomes for bone differentiation

Nahid Moradi<sup>1</sup>, Saeid Kaviani<sup>1\*</sup>, Mina Soufizomorrod<sup>1\*</sup>, Simzar Hosseinzadeh<sup>2,3\*</sup>, Masoud Soleimani<sup>2,1</sup>

<sup>1</sup>Hematology and Cell Therapy Department, Faculty of Medical Sciences, Tarbiat Modares University, Tehran, Iran

<sup>2</sup>Medical Nanotechnology and Tissue Engineering Research Center, Shahid Beheshti University of Medical Sciences, Tehran, Iran

<sup>3</sup>Department of Tissue Engineering and Applied Cell Sciences, School of Advanced Technologies in Medicine, Shahid Beheshti University of Medical Sciences, Tehran, Iran

## Article Info



### Article Type:

Original Article

### Article History:

Received: 27 Oct. 2021

Revised: 25 Dec. 2021

Accepted: 1 Jan. 2022

ePublished: 22 Aug. 2022

### Keywords:

PAA,  
 Tricalcium phosphate nanoparticles,  
 Freeze-drying,  
 Exosome,  
 Bone tissue engineering

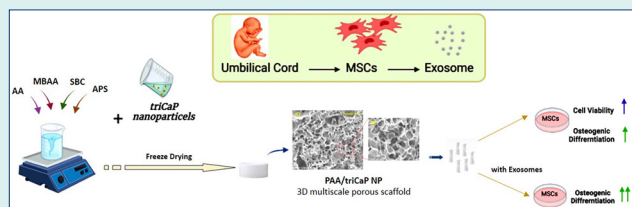
## Abstract

**Introduction:** This study focused on preparing a multiscale three-dimensional (3D) scaffold using tricalcium phosphate nanoparticles (triCaPNPs) in a substrate of poly(acrylic acid) (PAA) polymer for controlled release of exosomes in bone tissue engineering.

**Methods:** A scaffold was fabricated with a material mixture containing acrylic acid (AA) monomer, N,N'-methylenebisacrylamide (MBAA), ammonium persulfate (APS), sodium bicarbonate (SBC), and triCaPNPs called composite scaffold (PAA/triCaPNPs) via cross-linking and freeze-drying methods. The synthesis process was easy and without complex multi-steps. Through mimicking the hybrid (organic-inorganic) structure of the bone matrix, we here chose triCaPNPs for incorporation into the PAA polymer. After assessing the physicochemical properties of the scaffold, the interaction of the scaffold with human umbilical cord mesenchymal stem cells (UC-MSCs) such as attachment, proliferation, and differentiation to osteoblast cells was evaluated. In addition, we used DiI-labeled exosomes to verify the exosome entrapment and release from the scaffold.

**Results:** The polymerization reaction of 3D scaffold was successful. Based on results of physicochemical properties, the presence of nanoparticles in the composite scaffold enhanced the mechanical stiffness, boosted the porosity with a larger pore size range, and offered better hydrophilicity, all of which would contribute to greater cell penetration, proliferation, and then better bone differentiation. In addition, our results indicated that our scaffold could take up and release exosomes, where the exosomes released from it could significantly enhance the osteogenic commitment of UC-MSCs.

**Conclusion:** The current research is the first study fabricating a multiscale scaffold using triCaPNPs in the substrate of PPA polymer using a cross-linker and freeze-drying process. This scaffold could mimic the nanoscale structure and chemical combination of native bone minerals. In addition, our results suggest that the PAA/triCaPNPs scaffold could be beneficial to achieve controlled exosome release for exosome-based therapy in bone tissue engineering.



## Introduction

Bone repair in clinical therapy is still challenging which needs further research.<sup>1</sup> So far, although various methods have been developed for effective treatment to promote bone regeneration, such as conventional pharmacological treatments or grafting materials, the toxicity issues and

bioavailability limitations are still of concern.<sup>2</sup> On the other hand, autologous or allogeneic transplants have also failed to present an effective and satisfying treatment because of major disadvantages of these methods due to the secondary damage and immunological rejection of the transplant, respectively.<sup>3-6</sup>



\*Corresponding authors: Saeid Kaviani, Email: kavianis@modares.ac.ir; Mina Soufi-Zomorrod, Email: m.soufi@modares.ac.ir; Simzar Hosseinzadeh, Email: s.hosseinzadeh@sbmu.ac.ir



© 2023 The Author(s). This work is published by BioImpacts as an open access article distributed under the terms of the Creative Commons Attribution Non-Commercial License (<http://creativecommons.org/licenses/by-nc/4.0/>). Non-commercial uses of the work are permitted, provided the original work is properly cited.

In recent years, research on exosomes derived from mesenchymal stem cells (MSCs) has been an interesting way of examining paracrine factors and cell-to-cell communication,<sup>7,8</sup> since exosomes are essential bioactive mediators that are primarily responsible for the effects of MSCs on their surrounding microenvironment.<sup>9,10</sup> Umbilical cord (UC) is an endless and easily accessible MSC source.<sup>11</sup> Isolation of these cells does not require an invasive procedure; they multiply rapidly in the culture and are also said to be immune privileged.<sup>12,13</sup> Although several studies have reported the good impact of UC-MSCs in promoting bone repair,<sup>14-16</sup> few studies have focused on the effect of exosomes extracted from UC-MSCs in bone defect repair.

Thus, we used UC-MSCs to isolate exosomes. Since exosomes leave bone defect sites, it is important to use a suitable microenvironment for exosome entrapment.<sup>11</sup> Many efforts have been made to design 3D porous scaffolds to carry and release exosomes in a bone defect site.<sup>17,18</sup> Biocompatibility, good mechanical properties, and osteoconductive properties are the main features for scaffolds to ensure exosome function in the regeneration of bone defects.<sup>19,20</sup>

Recently, hydrogels have attracted much attention for therapeutic applications. Because of their high water content, chemical and physical properties, carbon-based network architecture, and presence of proper functional groups,<sup>21</sup> hydrogels have potential applications in tissue engineering,<sup>22</sup> and drug delivery.<sup>23</sup> So far, the hydrogel-based scaffolds that have been able to enhance osteointegration and differentiation in bone defects include engineered gels fabricated from natural compounds<sup>24</sup> as well as self-healing gels based on noncovalent cross-links.<sup>25</sup> Despite many advances in this field, there are some limitations with these hydrogel-based scaffolds, such as releasing toxic byproducts that are often accompanied by the formation of hydrogels, or complex and multi-step manufacturing process.<sup>2</sup>

Poly(acrylic acid) (PAA) is a synthetic polymer made from acrylic acid through controlled radical polymerization.<sup>26</sup> Because of their carboxylic groups, PAA-based polymers present a swelling tendency depending on environmental pH.<sup>21</sup> PAA-based polymers have almost all properties of a good pharmaceutical polymer, including biodegradable nature, nontoxicity, biocompatibility,<sup>27</sup> as well as great specific surface area, which would improve the interactions with physiological compartments.<sup>28</sup> They have applications as a scaffold for tissue engineering<sup>29,30</sup> and controlled protein or drug releasing in target tissues.<sup>21,31-35</sup> Zhao et al<sup>2</sup> engineered a hydrogel including nano-hydroxyapatite, sodium carbonate, and PAA. In that study, it was emphasized that the chelation between Ca<sup>2+</sup> and carboxylic groups of PAA was one of the reasons for the good scaffold stability.

Through mimicking the hybrid (inorganic-organic) structure of the bone matrix, we here chose tricalcium

phosphate nanoparticles (triCaPNPs) as the main inorganic compound of native bone mineral, for incorporation into PAA matrix.<sup>17,36-39</sup> Calcium phosphate (CaP) has been widely used as a bone substitute in clinical practice.<sup>40</sup> Apart from different phases, sizes, preparation, and formulation methods, in terms of application, CaP can be classified as nanoparticles (NPs), coatings, cement, and scaffolds.<sup>41</sup> Among all, calcium phosphate nanoparticles (CaPNPs) have shown good functional potentials in the field of nanomedicine. One of the great advantages of using CaPNPs is that these NPs are found in relatively high concentrations in the body, especially as the major constituent of bone and tooth enamel. They also have excellent biocompatibility, biodegradability, and osteoconductive properties.<sup>41</sup> However, pure NPs, because of their easy agglomeration and the instability of their suspension, cannot be used alone; so in the current study, we incorporated these NPs into the PAA polymer matrix.<sup>38,40,41</sup> Unlike many methods of synthesizing hydrogels, our synthesis process is straightforward and without complex or tedious steps. Based on the published article,<sup>42</sup> the present study aimed to fabricate a new scaffold formed from PAA and triCaPNPs via the freeze-drying process as a simple porous scaffold preparation method. Then, we explored the structural and mechanical properties of the scaffold, as well as the attachment plus differentiation of human UC-MSCs to osteoblast cells on the scaffold via *in vitro* study. Meanwhile, CaP biomaterials are only osteoconductive, not osteoinductive.<sup>43</sup> In this regard, previous studies have suggested that through adding these materials with bioactive proteins, growth factors, or osteogenic drugs, osteoinductivity to CaP biomaterials can be obtained.<sup>17,44,45</sup> Thus, considering the functional roles of exosomes in osteogenic differentiation, we carried exosomes (extracted from the UC-MSCs) with scaffold to evaluate osteogenic commitment of UC-MSCs. To the best of our knowledge, the current research is the first study to fabricate a nanocomposite scaffold formed from PAA and triCaPNPs to release exosomes for achieving accelerated bone differentiation.

## Materials and Methods

### Materials

All chemical reagents including acrylic acid (AA), triCaPNPs synthetic powder, nitric acid (HNO<sub>3</sub>) 65%, sodium bicarbonate (NaHCO<sub>3</sub>), sodium hydroxide (NaOH), ammonium persulfate (APS), paraformaldehyde, 4', 6-diamidino-2-phenylindole stain (DAPI), dimethyl sulfoxide (DMSO), tetrazolium salt (MTT), and Alizarin Red S (ARS) dye were purchased from Sigma-Aldrich, Germany. N, N'-Methylenebisacrylamide (MBAA) with CAS no:110-26-9 was purchased from Merk, Germany. DiI dye (CAS no: 41085-99-8) was purchased from Beyotime, China. BCA Protein Assay Kit was purchased from Bio Basic Inc., Canada. For cell culturing, reagents including phosphate-buffered saline (PBS), fetal bovine

serum (FBS), penicillin/streptomycin were purchased from Gibco, Invitrogen Corporation, USA. Trypsin/EDTA were purchased from Cegrogen Biotech GmbH, Germany. DMEM/F-12 (Dulbecco's Modified Eagle Medium/Nutrient Mixture F-12F) was purchased from Bioidea, Iran. Sterile deionized water was also used for all solutions.

#### **Cell isolation and identification of UC-MSCs**

Human UC samples were obtained after deliveries from the hospital with coordination and permission from the infants' parents, following the rules of medical ethics approved by the Faculty of Medical Sciences of Tarbiat Modares University. Near the placenta, the UC was cut into 1-1.5 cm pieces and washed several times with PBS and 2% penicillin/streptomycin. Thereafter, the fragments were exposed to 1 mL of collagenase enzyme (type II with a concentration of 0.014 g/mL) and were incubated at 37°C for 1 hour and vortexed every 10 minutes for 30 seconds. Then, FBS was added to neutralize collagenase, followed by centrifugation for 5 minutes at 400 g. The supernatant was removed and the cells were transferred to a 75 cm<sup>2</sup> flask (SPL Life Sciences) with DMEM/F12, 10% FBS, and 1% penicillin/streptomycin. After 72 hours, the medium was changed to remove debris and antibiotics. After observing the cell colonies, the cells were separated by 0.25% Trypsin-EDTA and transferred to 3 new 75 cm<sup>2</sup> flasks. To identify UC-MSCs, after removing the supernatant and washing with PBS, adherent cells in passage 3 were trypsinized to obtain 1×10<sup>6</sup> cells/mL, which were resuspended with PBS and centrifuged at 3000 rpm. After fixation with 4% paraformaldehyde and washing with PBS, the cells were exposed to antibodies (R&D Systems) CD73, CD90, CD105, CD34, CD45 and analyzed by FACSCalibur system (BD Biosciences, San Jose, CA, USA). For osteogenic induction, the cells were seeded. After reaching 70% confluence, the cells were treated with osteogenic differentiation medium (OM) containing DMEM/F12 + 10%FBS and bone differentiation factors: 50 mg/mL L-ascorbic acid-2-phosphate, 10 mM β-glycerophosphate and 0.1 nM of dexamethasone for 21 days. For adipogenic induction, the cells were cultured with DMEM/F12 + 10% FBS, 10 ng/mL insulin, and 10 nM dexamethasone for 21 days. The medium was changed twice per week for both adipogenic and osteogenic induction. The osteogenic and adipogenic differentiation was assessed using alizarin red and oil red O staining, respectively. Only UC-MSCs in passages 2 or 3 were used for all experiments.

#### **Preparation and characterization of scaffold**

Initially, at room temperature (RT) the mixed solutions of distilled AA (2.5 mL, 1.5 M) and MBAA (0.006 mol%) with NaOH (0.12 mol%) were made in 1 ml deionized water and placed on a magnetic stirrer (300 rpm, 30 minutes). In a separate container, 75 mg triCaPNPs was mixed with 5

mL deionized water and placed on a magnetic stirrer (250 rpm, 15 minutes). To enhance the solubility of NPs, 1.5 mL nitric acid 65% was added. Next, the main container was exposed to nitrogen gas to accelerate the polymerization process through removing oxygen. Under the nitrogen atmosphere, nanoparticle solution was added into the composite sample. Then, APS (0.012 mol%) was added as a radical initiator for the synthetic system of PAA and sodium bicarbonate (SBC, 0.02 mol%) as porogen in the PAA preparation, respectively.<sup>42</sup> The mixture of reactants was heated at 75°C to harden. Of note, all of these steps, except the addition of NPs, were performed to construct the bare scaffold as a control. The prepared samples were plunged in deionized water to remove any remained APS for 48 hours through refreshing deionized water at four-hour intervals. Then, the prepared samples were freeze-dried (Christ GAMMA 1-16 LSC Freeze Dryers, for 15 hours, -50°C).

#### **Structure and morphology characterization by FTIR and SEM**

Fourier transform infrared spectroscopy (FTIR) is a good analytical tool for identifying functional groups and characterizing covalent bonding information. FTIR spectra of the AA, PAA and PAA/triCaPNPs scaffolds were obtained using a FTIR spectrophotometer (FT-IR 8400S, Shimadzu, Japan) in the range of 4000–400 cm<sup>-1</sup>. The surface morphologies of scaffolds were observed by scanning electron microscopy (SEM, HITACHI S-4160 model) with an accelerating voltage of 30 KV and gold coating. The porosity percentage and surface pore size diameter of the scaffolds was recorded and then analyzed by ImageJ software (version 1.51j8). Four images from each scaffold were selected randomly and analyzed.<sup>46</sup>

#### **Swelling behavior**

The dried scaffolds were cut into 1 × 0.5 × 0.5 cm pieces. Dry weight was measured and recorded ( $W_d$  = dry state mass). These pieces were then immersed in PBS (pH = 7.4). At specific times, the samples were removed from the buffer and their weight was recorded after blotting the excessive buffer ( $W_s$  = swollen state mass).<sup>47</sup> Then the degree of swelling of the scaffolds was calculated using the following formula:

$$\text{Swelling degree} = \frac{W_s - W_d}{W_d}$$

#### **Mechanical test**

The mechanical (compressive) properties of the scaffolds were assessed using a universal mechanical analyzer (Zwick Roell). Cylindrical-shaped scaffolds with approximately 15 mm in diameter and 10 mm in height were compressed (constant speed of 0.5 mm/min).

#### **Water contact angle assay (WCA)**

To know the hydrophilicity of the constructed scaffolds, the contact angle was measured at room temperature using a G10 Kruss contact angle goniometer. This test was performed by adding 10 μL deionized water droplet

on the freeze-dried scaffolds surface and then analyzed by ImageJ DropSnake plugin.

### Investigation of cell attachment

DAPI staining was used to evaluate the attachment of MSCs onto the constructed scaffolds and to confirm the growth plus viability of the cells over time. For this purpose, first the scaffold pieces were sterilized with 70% ethanol and UV radiation and then the culture medium was poured onto the scaffolds in each well of the plate and incubated at 37°C with 5% CO<sub>2</sub>. After 24 hours and confirming that the scaffolds were not contaminated,  $5 \times 10^5$  cells/cm<sup>2</sup> were seeded on the scaffolds. The cells were refreshed every 3 days with DMEM/F12 +10% FBS. On days 3 and 21 after cell seeding, the cells were washed once with PBS after which DAPI (dilution 1:1000) was exposed to the cells for 4-6 minutes. The results were observed by Olympus iX53 microscope (Olympus Corporation). For SEM, the cells were fixed with glutaraldehyde 4% and then dehydrated with alcohol serial 50%, 60%, 70%, 80%, 90%, and 100%, respectively, (10 minutes for each).

### UC-MSCs viability on scaffold

Cell survival and proliferation were determined using MTT. MSCs were seeded on bare and composite scaffolds (3D) in a 96-well plate with  $2 \times 10^4$  cells/well. UC-MSCs cultured on plate (2D) and scaffolds without any cells were used as controls. At time points, MTT solution was added to each well and incubated at 37°C for 4 hours. Thereafter, DMSO was added to each well to dissolve the formed formazan crystals. Due to the hydrophilic properties of the scaffolds, the penetration of cells into the scaffold was predicted. Thus, in the group of scaffold+cells, in order to completely empty the cells from the scaffold, after the mentioned steps, the scaffolds were into smaller pieces and all contents of the wells were transferred into a clean microtube with a glass bead. Then, the microtube was vortexed for 3 to 5 minutes. The glass bead hit the scaffolds to release the cells from the scaffolds. Absorbance readings were performed at 570 nm.

### Cell differentiation assays

To show the impact of scaffolds on osteogenic differentiation, UC-MSCs were seeded on PAA and PAA/triCaPNPs scaffolds (3D). Once grown to 70% confluence, the cells were treated and refreshed every 3 days with OM.

### UC-MSCs mineralization on the scaffolds

To indicate the mineralization after 21 days of bone induction of UC-MSCs seeded on PAA and PAA/triCaPNPs scaffolds, the cells were fixed and dried, after which their surface and cross-section were observed by SEM.

### Alizarin red staining (ARS) analysis

After 14 and 21 days of osteoinduction culture, the samples were fixed (10% formalin, 15-20 minutes), and then washed with PBS. The fix cells were covered in ARS (2% w.t/v, pH=4.2, 10 min). Once washed, the samples were observed under Olympus iX53 microscope. To quantify the coloration of ARS, the samples were incubated for 18 h with an added 10% acetic acid, and transferred to microtubes for centrifugation (20000 g, 15 minutes). Then, 10% ammonium hydroxide for neutralization was added to the supernatant. Finally, 100 µL of each sample was added to 96-well plates and absorbance readings were performed at 405 nm.<sup>48</sup>

### Alkaline phosphatase (ALP) activity assay

The ALP activity was measured using ALP Assay kit (Man Company, Tehran, Iran) after 7 and 14 days of osteoinduction based on the manufacturers' protocols. Total protein extraction was performed using RIPA lysis solution. Then, the activity of ALP in the cell lysates was calculated at 405 nm and the data were normalized against total proteins.

### Quantitative real-time PCR (RT-qPCR) analysis

Total RNAs were isolated using TRIzol reagent (Geneall, Korea) based on the manufacturer's instructions on days 14 and 21 after osteoinduction with cDNA synthesized using cDNA synthesis kit (BioFACT Co., Korea). RT-qPCR was performed using SYBR Green Master Mix (Applied Biosystems, USA) and StepOne Real-Time PCR System (Applied Biosystems, USA). The sequence gene primers<sup>46</sup> are reported in Table 1. Results were normalized with GAPDH.<sup>17</sup>

### Extraction and Identification of Exosomes

Initially, we needed exosome-free FBS (depleted of exosomes which was obtained by FBS ultracentrifugation at 100 000 g for double 2 hours) to separate the exosomes. UC-MSCs were seeded in 175 cm<sup>2</sup> flasks and after reaching a density of more than 80%, their supernatant was replaced with 10% exosome-free FBS and DMEM. Every 48 hours, the cell surface medium was collected

**Table 1.** Sequences of the primers

Gene	5'-3'(Forward)	5'-3'(Reverse)
Collagen Type I (COL1α1)	TTGTGGATGGGGACTTGTGA	AGAGGCAGGTGGAGAGAGG
Alkaline phosphatase (ALP)	CAACAGGGTAGATTTCTCTTGG	GGTCAGATCCAGAATGTTCC
RUNX2	TCTTAGAACAAATTCTGCCCTTT	TGCTTTGGTCTTGAATCACA
Osteocalcin (OSC)	CCAAGGAGGGAGGTGTGTGAG	AAGGGGAAGAGGAAAGAAGGGTG
GAPDH	GCAGGGATGATGTTCTGG	CTTTGGTATCGTGAAGGAC

and centrifuged (300 g, 10 minutes; 2000 g, 10 minutes; and 10000 g, 30 minutes) to remove cells and cell debris. Then, the supernatant was filtered (a 0.22  $\mu\text{m}$  sterile filter) and then ultracentrifuged (100000 g, 70 minutes). Next, the supernatant was removed and after washing the pellet with PBS, it was again ultracentrifuged to get exosomes.<sup>49</sup> Exosome protein concentrations were evaluated with the Pierce BCA Protein Assay Kit (Bio Basic Inc., Canada) according to the manufacturer's protocol. Transmission electron microscopy (TEM, Leo 906, Germany) was used to observe the morphology of the exosomes. The size distribution of the exosomes was captured via dynamic light scattering (DLS) by a Nanotracer Wave II (Microtrac, Inc.) Analysis of exosomal surface markers such as CD9 and CD81 (Abcam, USA) was also performed through Western blotting. UC-MSCs were used as control.

#### *Effects of exosomes on UC-MSCs proliferation*

In this step, we evaluated the effects of UC-MSCs-derived exosomes on proliferation of their parent cells. The cells were treated with two concentrations of exosomes (25 and 50  $\mu\text{g}/\text{mL}$ ). MTT and DAPI staining were performed. Based on a study conducted by Yang et al.,<sup>11</sup> we selected the minimum concentration of exosomes. So only 25  $\mu\text{g}/\text{mL}$  exosome was used to evaluate bone differentiation.

#### *Release and internalization of exosomes*

The release of exosomes from the bare and composite scaffolds was calculated according to Yang et al.<sup>11</sup> Briefly, the exosomes seeded drop by drop onto the surface of scaffolds at a density of  $6 \times 10^{10}$  particles/mL and placed in a humid incubator for 24 hours for the exosomes to be totally absorbed. Then, the combinations of exosome/bare scaffold and exosome/composite scaffold were placed in PBS (pH= 7.4) at 37°C. The supernatants were collected for 2 weeks to compute the amount of exosome/release by BCA protein assay Kit. Also, we used DiI-labeled exosomes to show penetration of exosomes into UC-MSCs. DiI dye was used according to the manufacturer's protocol. Labeled exosomes, seeded onto the surface of scaffolds. Then the exosome-enriched scaffolds were exposed to UC-MSCs with about 70% confluence in 6-well plate. After culturing for 18 hours, the exosome/scaffold combinations were removed. Next, the cells were washed with PBS and fixed with paraformaldehyde and stained with DAPI solution.<sup>18</sup> The results were observed using Olympus iX53 microscope.

#### *Effects of exosomes on UC-MSCs commitment*

To evaluate the performance of exosomes released from scaffold and their impact on osteogenic commitment of UC-MSCs *in vitro*, the combinations of exosome/scaffold were prepared as described above and placed in a well culture plate. Next, UC-MSCs were seeded inside the same well plate and treated with OM until the cells come together compactly (nearly 70 hours).<sup>18</sup> After culturing,

the scaffolds or exosome/scaffold combinations were removed. Then, total RNAs of UC-MSCs were isolated and the gene expression of some biochemical markers for osteogenesis (collagen type I, ALP, RUNX2 and osteocalcin) was evaluated by RT-qPCR. Relative levels of gene expression were normalized by GAPDH.

#### *Data analysis*

Either one or two-way ANOVA analysis or t-test was used to determine the difference between results. All data presented in this study have been represented as mean  $\pm$  standard deviation of at least three replicates of each sample. GraphPad Prism was used for data analysis.  $P < 0.05$  was considered statistically significant.

## **Results**

### *Identification and characterization of UC-MSCs*

MSCs isolated from the UC were spindle-shaped. Flow cytometry results revealed that the cells expressed mesenchymal CD markers (CD73 and CD90, CD105) while they did not express CD45 and CD34. In addition, as displayed in Fig. 1, these cells could differentiate into osteoblasts and adipocytes.

### *Physicochemical features of 3D scaffolds*

*FTIR:* PAA/ triCaPNPs (composite) and PAA (bare: as control) scaffolds were prepared via cross-linking and freeze-drying process. To investigate the structure of the fabricated scaffolds, FTIR was used; as can be seen in the Fig. 2A, the PAA sample revealed a clear peak at  $3600\text{ cm}^{-1}$ , which was not observed in its monomer. This emphasizes that the synthesis of PAA was performed successfully. On the other hand, in the area  $2600\text{ cm}^{-1}$  to  $3000\text{ cm}^{-1}$  a wide peak with a center of  $2970\text{ cm}^{-1}$  was observed in both synthesized scaffold samples, suggesting the presence of CH<sub>2</sub>, CH, and CH<sub>3</sub> groups in them. Compared with the FTIR spectrum of acrylic acid monomer, the displacement or disappearance of some peaks in the synthesized polymer samples confirms its successful synthesis. In the PAA spectrum, we observed the removal of the peak characteristic of the tensile vibration H in the group CH<sub>2</sub>=CH-COOR at  $3060\text{ cm}^{-1}$  (which is observed only in the monomer spectrum), which also confirmed its successful synthesis. Also, the peaks observed in the monomer, which were within the range of  $1500\text{--}1900\text{ cm}^{-1}$ , were merged after polymer synthesis, and only two characteristic peaks appeared at  $1570\text{ cm}^{-1}$  and  $1730\text{ cm}^{-1}$ , indicating the C=O vibration. This also reflected the synthesis of PAA and the efficiency of the synthesis method. Also, in the FTIR spectrum of the composite, the observation of the peak at  $1540\text{ cm}^{-1}$  wavelength confirmed the proper interaction of PAA and Ca<sup>2+</sup> ions through electrostatic interactions.

*SEM:* In order to determine the scaffold morphology, PAA and PAA/triCaPNPs scaffolds cross-sectional thickness were prepared and observed by SEM and

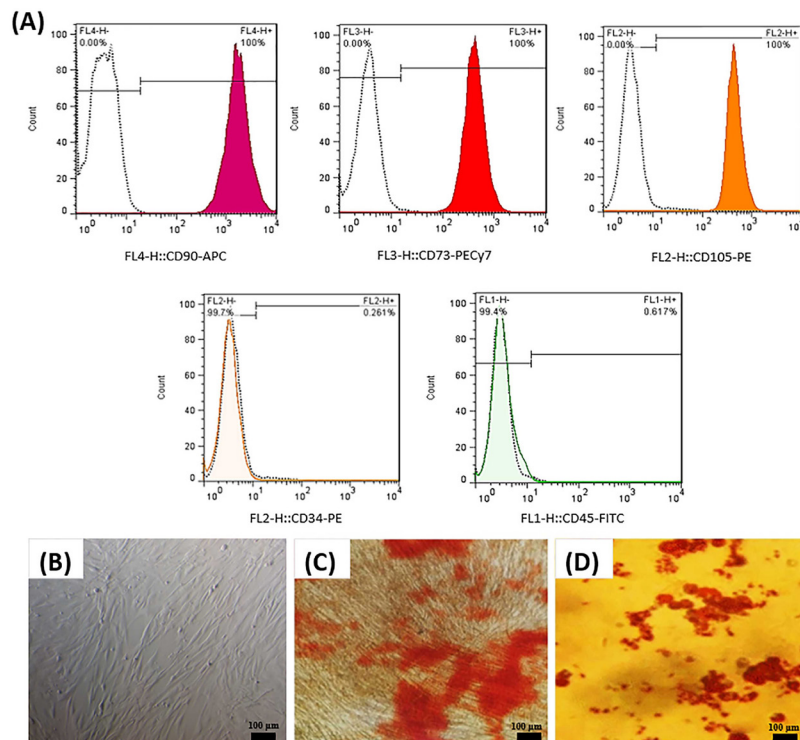


**Fig. 1.** Identification of UC-MSCs. Flow cytometry analysis of UC-MSCs surface CD markers expression (A). UC-MSCs monolayer at approximately 70% confluence in Passage 3 (B). UC-MSCs stained by alizarin red after 21 days culturing in osteogenic medium (C). UC-MSCs stained by oil red O after 21 days culturing in adipogenic medium (D).

analyzed using ImageJ software. According to the analysis, both scaffolds revealed an interconnecting 3D multiscale pore architecture. In addition, PAA scaffold had pores with 5-80 µm diameter and 55.2% porosity, while the pore diameter of PAA/triCaPNPs scaffold was 3-120 µm with

68.3% porosity (Fig. 2B).

*Swelling degree:* The swelling properties of scaffolds are shown in Fig. 2C. According to the results, the swelling ratios of the scaffolds grew over time. PAA and PAA/triCaPNPs reached the equilibrium swelling at

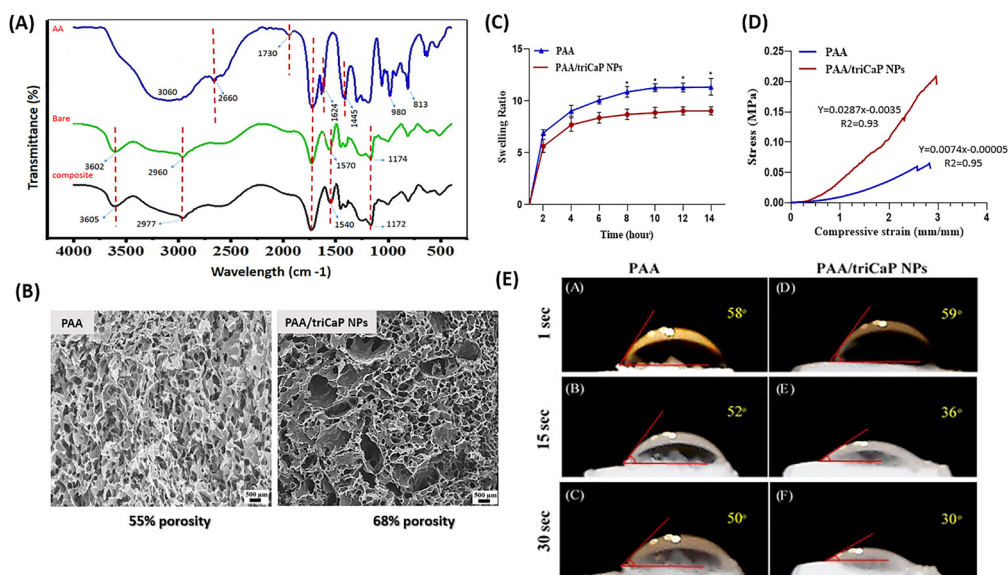


**Fig. 2.** Physicochemical properties of fabricated scaffolds. FTIR absorbance spectra of acrylic acid monomer (blue line), PAA (green line) and PAA/triCaPNPs (black line) scaffolds (A). SEM analysis of cross-section morphology of porous structure of scaffolds. The scale bars represent 300 µm. PAA and PAA/triCaPNPs show 55.2% and 68.3% porosity, respectively (B). Swelling properties of scaffolds at different time points, (n = 3) (C). Representative compressive stress-strain curves of scaffolds, (n = 3) (D). Water contact angle measurements on the freeze-dried PAA (A-C) and PAA/triCaPNPs (D-F) scaffolds at 1, 15, and 30 seconds after starting the test (\**P*<0.05) (E).

approximately 10 hours. The swelling ratio was observed higher in bare scaffold.

**Compression test:** The results of compression test of the constructed scaffolds in Fig. 2D indicated that the PAA/triCaPNPs and PAA scaffolds could withstand a maximum of 0.209 MPa and 0.065 MPa, respectively. Thus, it seems by adding triCaPNPs the stiffness of the scaffold increased.

**Water contact angle (WCA):** The hydrophilic properties of scaffolds were defined using WCA (Fig. 2E). As displayed in the first second after starting the test, the angle formed between PAA scaffold and water drop was 58° and between PAA/triCaPNPs scaffold and water drop was found 59°, while at 30 seconds after initiating the test, the contact angles were 50° and 30°, respectively, which shows that the presence of NPs within the PAA matrix boosted the hydrophilicity of the prepared composite scaffold.

### Survival rate of UC-MSCs and attachment characterization on scaffolds

To evaluate the attachment and growth of UC-MSC on the scaffolds, DAPI staining and SEM images were used on days 3 and 21 after cell seeding on both scaffolds. Fig. 3A clearly showed that the cells were attached to the surface of the scaffolds and grew as well as proliferated on them. MTT assay results confirmed that the cell viability rate was very good during the culture period and none of the scaffolds were toxic for UC-MSC (Fig. 3B).

### Effect of scaffolds on osteogenic differentiation of UC-MSCs

The matrix mineralization of UC-MSCs on the PAA and PAA/triCaPNPs scaffolds in osteogenic medium was

evaluated using SEM on day 21. As can almost be deduced from the micrographs, mineral depositions produced by MSCs, filled the scaffolds pores in both groups, but it seems that the secretion of the bone matrix by UC-MSCs attached on the composite scaffold was far higher (Fig. 4). ARS as histological staining identifies calcium mineralization by osteoblasts.<sup>2</sup> As depicted in Fig. 5A-B, compared with UC-MSCs cultured on the bare sample and 2D culture as controls, more calcium deposition was detected when the cells were cultured on the composite scaffold. This result confirmed the promoting role of CaPNPs in bone mineralization ( $P < 0.001$ ). After 7 and 14 days of osteogenic induction, evaluation of ALP enzyme activity showed that the activity of this enzyme increased on day 14 in Cell+PAA/triCaPNPs group compared with 2D culture and Cell+PAA groups (Fig. 5C,  $P < 0.01$ ). Consistent with the results of ALP activity and ARS, real-time qPCR analysis also indicated that the mRNA expression of bone differentiation marker genes in Cell+PAA/triCaPNPs group was significantly higher than 2D culture and Cell+PAA groups (Fig. 5D-F).

### Characterization of exosomes extracted from UC-MSCs

After isolating the exosomes by an ultracentrifuge, their average size was captured using DLS and their morphology was analyzed by TEM. The size distribution of the exosomes was within 45-105 nm (Peak = 55 nm). Exosomes were observed in a round and membrane form in TEM images (Fig. 6A-B). BCA Protein Assay indicated that isolated exosome concentration was 100 µg/mL. Western blot analysis confirmed that exosomes derived from UC-MSCs were positive for the exosome specific markers CD9 and CD81 (Fig. 6C).

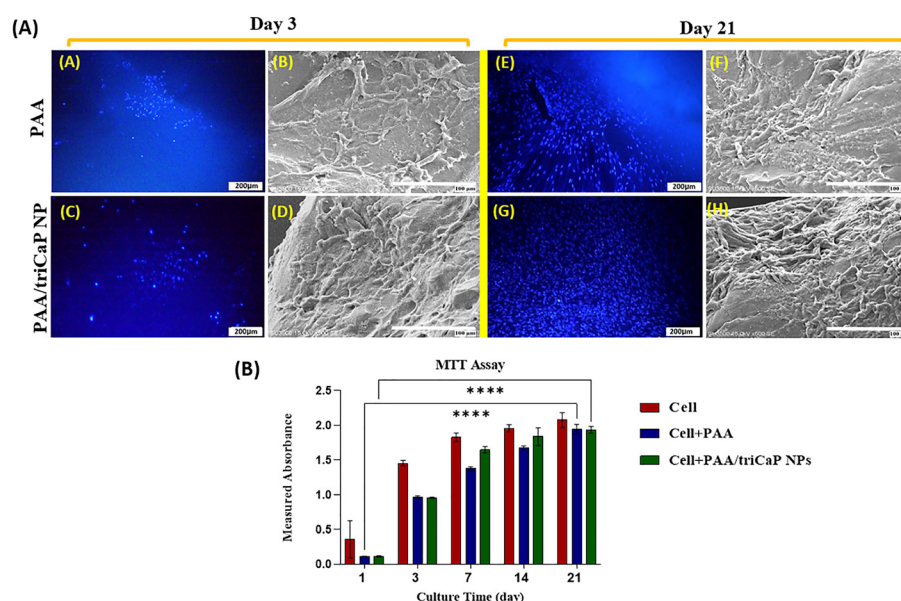


**Fig. 3.** Cell attachment analysis on PAA and PAA/triCaPNPs scaffolds through DAPI staining (A, C, E, G; scale bars: 200 µm) and SEM images (B, D, F, H; scale bars: 100 µm) on days 3 and 21 of the culture period in DMEM/F12 (a). Cell viability on scaffolds (3D culture) and plate (2D culture: cells) on days 1, 3, 7, 14, and 21, (n = 4) (\*\*\*\* $P < 0.0001$ ) (b).

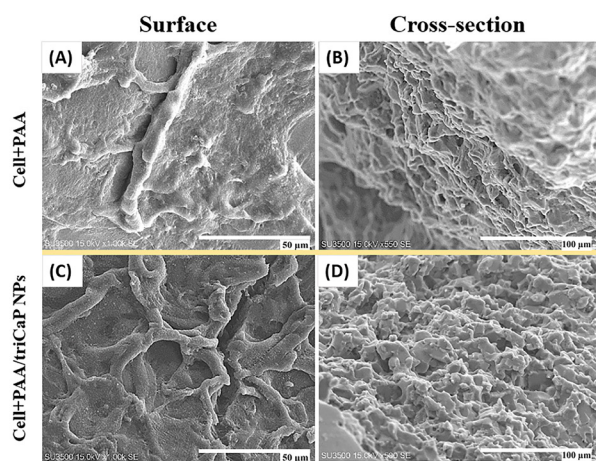


**Fig. 4.** SEM photograph of UC-MSCs mineralization on the scaffolds in the osteogenic medium on day 21. The surface of scaffolds at 50  $\mu\text{m}$  scale (A, C) and cross-section of scaffolds at 100  $\mu\text{m}$  scale (B, D) were imaged. UC-MSCs filled the scaffold pores with mineral deposition, especially in Cell+PAA/triCaPNPs group.

#### Effects of exosomes on proliferation of UC-MSCs

In this step, we checked the effects of exosomes derived from UC-MSCs on proliferation of their parent cells. The cells were treated with two concentrations of exosomes (25 and 50  $\mu\text{g}/\text{mL}$ ). The results of the MTT assay revealed that higher concentration of exosomes led to greater proliferation of UC-MSCs. Meanwhile, the effects of exosome concentrations were not significant on the first day but significant on days 3 and 7. In addition, DAPI staining on day 7 confirmed MTT results (Fig. 6D-F). Based on a study conducted by Yang et al,<sup>11</sup> we selected the minimum concentration of exosomes. So only 25  $\mu\text{g}/\text{mL}$  exosome was used to evaluate bone differentiation.

#### Assessment of exosome release and internalization by UC-MSCs

DiI-labeled exosomes were used to show exosome entrapment in both fabricated scaffolds. As displayed in Fig. 7, the red-labeled vesicles are present on the surfaces of both scaffolds showing the ability of the exosomes to be connected with the scaffolds surface. By using BCA protein assay kit, the release profiles of exosomes from both scaffolds was captured for 2 weeks and indicated as two curves (Fig. 8A). Specifically, 68.2% and 80.3% of the exosomes were released from the composite and bare scaffolds, respectively ( $P < 0.05$ ). The penetration of exosomes released by the scaffolds into UC-MSCs was detected for 18 h after incubating the DiI-labeled exosomes/scaffolds combination with UC-MSCs. Afterwards, the cells were fixed and stained with DAPI. As depicted in Fig. 8B, exosome uptake was confirmed by UC-MSCs.

#### Effects of exosomes on osteogenic commitment of UC-MSCs

To evaluate the function of exosomes released from scaffolds and their impact on osteogenic commitment of UC-MSCs *in vitro*, the gene expression of some specific markers for osteogenesis was evaluated by RT-qPCR. The cells incubated in the presence of composite scaffold significantly enhanced the expression of collagen type I, ALP, RUNX2, and osteocalcin ( $P < 0.05$ ), though in the presence of exosomes-enriched composite scaffold, the expression was far higher ( $P < 0.01$ ). No statistical significance for Cell, Cell+Exo, and the bare scaffold was observed (Fig. 9).

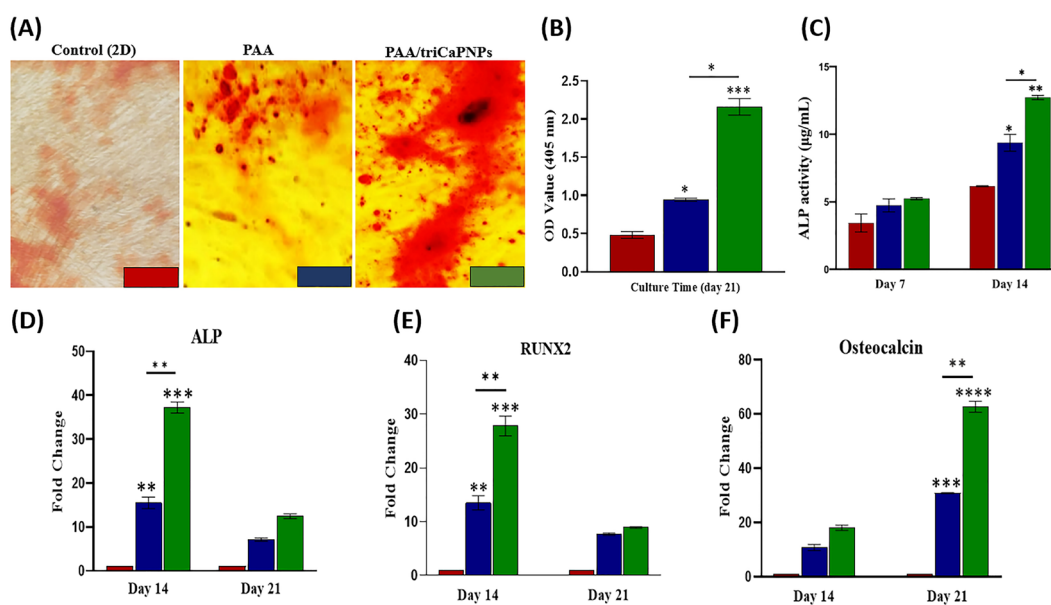


**Fig. 5.** Effect of scaffolds on osteogenic differentiation of UC-MSCs. Alizarin Red S staining on 21 days after osteogenic induction in 2D and 3D cultures (A). The quantitative analysis of ARS on day 21, ( $n = 3$ ) (B). ALP activity of UC-MSCs attached on PAA and PAA/triCaPNPs 3D scaffolds and 2D culture on days 7 and 14 (C). Expression of bone differentiation marker genes was measured by RT-qPCR on days 14 and 21: Alkaline Phosphatase (D) and RUNX2 (E) as early markers; Osteocalcin (F) as a late marker. Results were normalized by GAPDH ( $n = 3$ ) ( $P < 0.05$ )

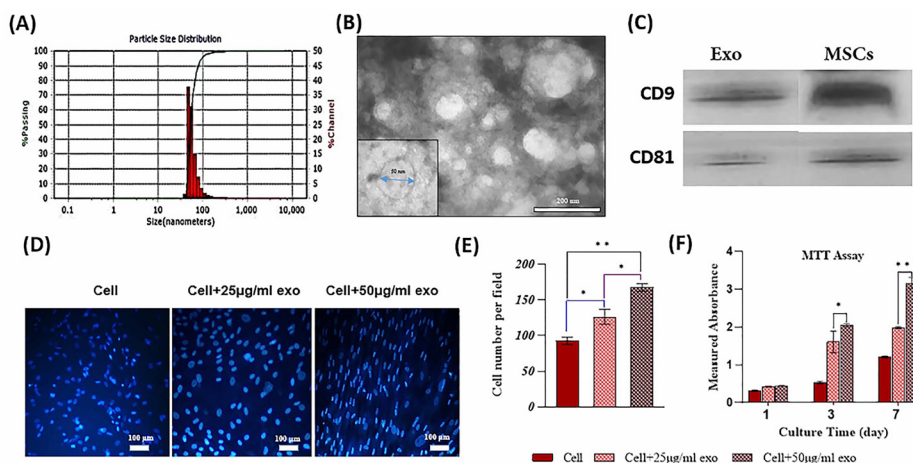


**Fig. 6.** Characterization of exosomes derived from human UC-MSCs. Representative results of DLS (A). TEM photograph of the exosomes (B). Analysis of western blotting of exosome specific markers (CD9 and CD81) (C). Effect of exosomes on the proliferation of UC-MSCs: MTT assay results (D). DAPI staining results after 7-day incubation of UC-MSCs with two concentrations of exosomes (E). Quantitative analysis of DAPI staining. ( $n = 3$ ) (\* $P < 0.05$ , \*\* $P < 0.01$ ) (F).

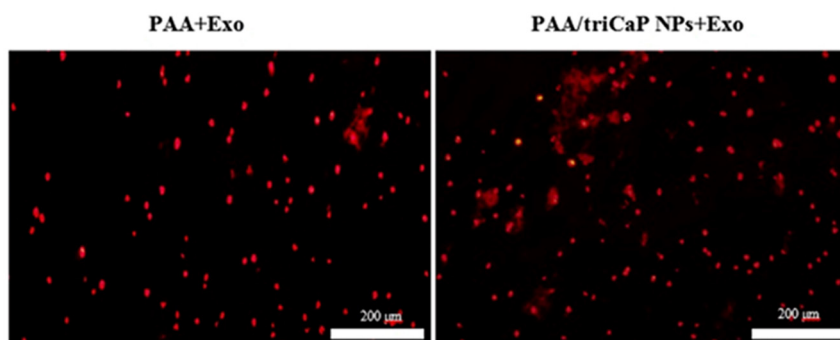


**Fig. 7.** Red labeled-exosomes attached on PAA (left) and PAA/triCaPNPs (right) scaffold surfaces; scale bars: 200  $\mu\text{m}$ .

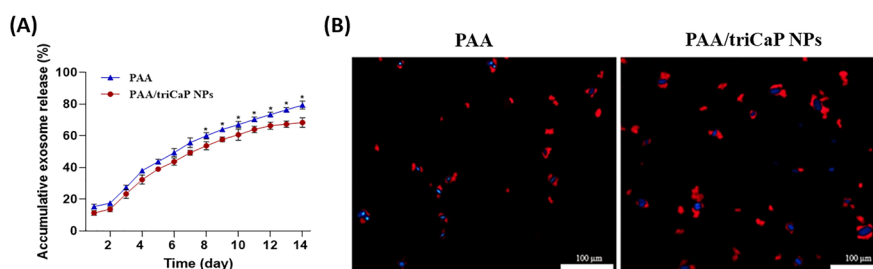


**Fig. 8.** Exosome release assessment. Release curve of exosomes from the bare and composite scaffolds, ( $n = 3$ ) (\* $P < 0.05$ ) (A). Ingestion of exosomes. The red Dil-labeled exosomes/scaffolds combination incubated with UC-MSCs for 18 h. Then, the nuclei of UC-MSCs were stained using DAPI (blue); scale bars: 100  $\mu\text{m}$  (B).

## Discussion

This study aims to create a biocompatible substrate that is able to fill a bone defect site, consisting of osteoconductive material, and contributing to the gradual release of exosomes as a repair-guiding factor.<sup>50</sup> In this study, as the first step, a scaffold was fabricated with a material mixture containing AA monomer, MBAA as crosslinker, and triCaPNPs powder (PAA/triCaPNPs: composite) via

the freeze-drying method. The synthesis process was easy, straightforward, and without containing complex multi-steps. We chose CaPNPs to improve the physicochemical properties of PAA to develop a new option for bone repair engineering. To investigate the effect of the presence of NPs in the scaffold, one sample without NPs (PAA: bare) was used in all experiments.

Since the PAA has a plenty of negative charge due to

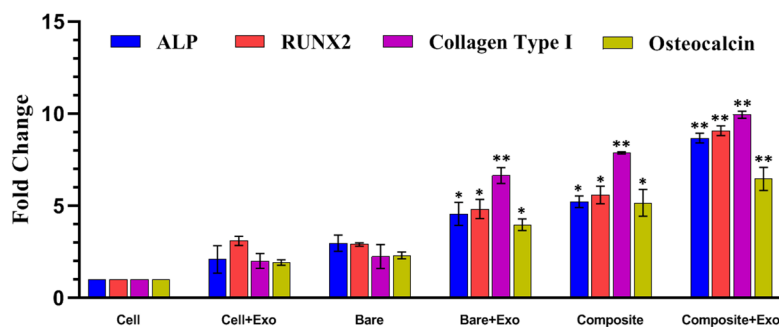


**Fig. 9.** Effect of exosomes released from scaffolds on the expression of bone commitment marker genes of UC-MSCs seeded on monolayer in 2D culture. All groups were in OM, (n =3) ( $P < 0.05$ ). NOTE: *Cell group*: UC-MSCs without any exosome or scaffold; *Cell+Exo group*: 25  $\mu\text{g/mL}$  exosome was added directly to UC-MSCs; *Scaffold group*: bare or composite scaffolds were placed in a well culture plate; *Scaffold+Exo group*: The combinations of exosome/scaffold were prepared and placed in a well culture plate. Then UC-MSCs seeded inside the same well plate until the cells come together compactly (nearly 70 hours).

carboxylic groups<sup>51</sup> and CaPNPs have a positive charge because of the presence of  $\text{Ca}^{2+}$  on their surface,<sup>52</sup> PAA was predicted to cross-link together with CaPNPs via electrostatic bonding. The FTIR results also showed the same. Based on FTIR results, the peak of H vibration in the C=C-H group at  $980\text{ cm}^{-1}$  of the monomer was weakened after the synthesis of the bare (or composite) scaffold.<sup>53,54</sup> The peak at  $1172\text{ cm}^{-1}$ , which is related to the C-C tensile vibration in the synthesized sample, also proved that the PAA polymerization reaction was successful. The observation of the peak at  $1540\text{ cm}^{-1}$  wavelength in the FTIR spectrum of the composite scaffold confirmed the proper interaction of PAA and  $\text{Ca}^{2+}$  ions through electrostatic interactions. In addition, the absence of peak phosphate group ( $\text{PO}_4^{3-}$ ) characteristics in the FTIR composite spectrum (at  $1020\text{ cm}^{-1}$  and  $1060\text{ cm}^{-1}$ ) was another reason for proper interaction between tricalcium phosphate particles and functional groups on the PAA surface.<sup>55</sup>

MBAA and SBC function cooperatively to induce the porosity.<sup>56</sup> In our study, SEM analysis confirmed a 3D, multiscale porous, and interconnected porous morphology of the scaffolds. The porous structure of bare and composite scaffolds appeared with 55.2% and 68.3% porosities, plus  $5\text{-}80\mu\text{m}$  and  $3\text{-}120\mu\text{m}$  pore sizes, respectively. It showed that the presence of NPs has a positive effect on creating more porosity and a larger range of pore size. The continuous channels on these scaffolds could mimic the nanoscale building design of native bone minerals which would ameliorate the osteoconductive capability, which is fundamental for promoting cell attachment, migration, proliferation, and differentiation.<sup>57</sup> Further, micronutrients can be directed through interconnected porosity.<sup>41</sup> Based on previous findings, scaffold pore size and porosity are related to the surface area available for cell adhesion plus cell growth,<sup>1</sup> which have also been shown to promote osteogenic differentiation<sup>58</sup> and osteogenesis.<sup>59</sup> In the literature, a range of pore sizes is considered as optimal sizes in a bone scaffold: for new functional microvascular networks it is  $5\text{ }\mu\text{m}$ , for osteoid ingrowth is  $40\text{-}100\text{ }\mu\text{m}$ , and for bone

regeneration  $100\text{-}350\text{ }\mu\text{m}$ .<sup>1</sup> Thus, the composite scaffold has all recommended pore sizes in comparison with the bare sample to osteogenic differentiation of UC-MSCs.

The Young's modulus values of PAA and PAA/triCaPNPs scaffolds were obtained approximately 0.007 and 0.028 MPa, respectively. So, according to the mechanical test results, higher stiffness was observed through incorporating the triCaPNPs. Moreover, we recorded the water contact angle of both scaffolds, as the wettability property of the scaffold plays a fundamental role in their interaction with different cells.<sup>60</sup> According to the WCA measurement, the presence of NPs in the structure of the composite scaffold elevated its wetting rate. Thus, the nanocomposite scaffold would have a harder structure along with more hydrophilicity. The hydrophilic scaffolds are simply wetted in a culture medium and can cause better cell migration and adhesion.<sup>61</sup>

The swelling ratio of fabricated scaffolds was evaluated through checking their wet weight changes in PBS at  $37^\circ\text{C}$  (physiological condition). The results revealed that the presence of NPs in the structure of the composite scaffold caused a lower swelling rate than the bare sample. In this regard, Hosseini et al<sup>62</sup> also found the same results. They prepared PAA/xanthan gum/graphene oxide and indicated that hydrogels with NPs have a lower swelling percentage. Since the swelling behavior depends on chemical and physical properties of fabricated scaffolds,<sup>63</sup> according to previous findings,<sup>64</sup> in the presence of  $\text{Ca}^{2+}$ , the swelling quantity of PAA diminishes, because of strong hydrogen interactions of  $\text{Ca}^{2+}$  in NPs with free carboxylic groups in the scaffold.

After evaluating the physicochemical properties of the scaffolds, as the second step, to verify the biocompatibility of scaffolds, UC-MSCs were successfully isolated, characterized, and seeded on both samples. Consistently, all results related to the MTT assay, SEM analysis and, DAPI staining confirmed good biocompatibility of the scaffolds.

Fabrication of a scaffold with suitable mechanical and osteogenic properties was one of the purposes of this study. Thus, we chose triCaP and to attain good

dispersion ability in the PAA matrix, we added the nanoparticle form of triCaP. Subsequently, the osteogenic properties of the scaffolds were investigated. Generally, in all tests related to evaluating the osteogenic properties of scaffolds, UC-MSCs cultured on both scaffolds (3D culture) showed more osteogenic properties compared with the cells cultured on the plate (2D culture). Even the 3D microenvironment provided by the bare scaffold could help in better cell differentiation compared with the 2D culture. By comparing the two fabricated scaffolds, triCaPNPs can be considered responsible for the better performance of the composite scaffold in UC-MSCs osteogenic differentiation. Previous studies demonstrated that bone regeneration is facilitated by CaPs, through regulating the activation of osteoblasts-osteoclasts and promoting bone mineralization via secretion of calcium and phosphorus ions.<sup>65</sup> Here, we have shown two important roles of triCaPNPs: 1) improving the physicochemical properties of PAA polymer such as mechanical stiffness, greater porosity with a larger pore size range, and better wetting properties, all of which can contribute to better cell penetration and differentiation; 2) enhancing the bone differentiation of UC-MSCs cultured on the composite scaffold.

As the next step in this study, after isolating the exosomes, to answer the question whether the scaffolds can trap and release exosomes for usage in bone repair applications, we first assessed the effects of two concentrations of exosomes on the proliferation of UC-MSCs. The results indicated that exosomes can significantly improve proliferation of cells in a dose-dependent manner which was similar to previous studies.<sup>11,17</sup> To control the consumption of exosomes and based on Yang et al,<sup>11</sup> we selected 25 µg/mL to evaluate bone differentiation. After that, we incubated DiI-labeled exosome/scaffolds combination with the cells for 18 hours to detect whether the exosomes can ingest by UC-MSCs.<sup>18</sup> As Fig. 7 and Fig. 8 showed that the exosomes were successfully trapped in scaffold surfaces as well as exosomes released from the scaffolds and ingested by UC-MSCs.

Since there is evidence demonstrating the beneficial effects of exosomes on bone repair,<sup>66,67</sup> various studies have been performed to compound exosomes with materials to help prolong the presence of exosomes at the site of bone defects. Zhang et al<sup>17</sup> combined exosomes (derived from human-induced pluripotent stem cells) with β-TCP to repair calvarial bone defect model, but exosomes were entirely released after 5 days *in vitro*. Li et al<sup>68</sup> prepared PLGA/pDA scaffolds formed from PLGA scaffolds with polydopamine (pDA) to achieve slow release of the exosomes derived from human adipose-derived stem cells. Nearly, 70% of exosomes were released from the scaffold after 8 days *in vitro*. Yang et al<sup>11</sup> prepared an injectable hydroxyapatite-embedded hyaluronic acid-alginate (HA-ALG) hydrogel. They showed approximately 71.2% of the exosomes derived from UC-MSCs were released from

## Research Highlights

### What is the current knowledge?

- √ PAA is an anionic synthetic polymer.
- √ triCaPNPs have excellent biocompatibility and osteoconductive properties.

### What is new here?

- √ A novel 3D multiscale scaffold prepared from triCaPNPs in a substrate of PPA polymer.
- √ triCaPNPs improve the physicochemical properties of PAA polymer that are in favor of osteogenic differentiation.
- √ PAA/triCaPNPs scaffold can carry and release exosomes in functional form into the medium.

the material after 2 weeks. In our current study, after 2 weeks of continuous evaluation, the composite scaffold had a slower release effect (68.2%) on exosomes compared with the bare one (80.3%) ( $P < 0.05$ ). It was previously demonstrated that the higher swelling ratio in bare scaffold was caused by the faster exosome releasing from it,<sup>11</sup> as also confirmed by our results.

In addition, UC-MSCs cultured in the presence of composite scaffold revealed the highest expression of osteogenic markers, particularly in the presence of exosome-enriched composite scaffold, indicating that the bioactivity of scaffold components plays a stimulating role in gene expression. In this study, we observed that the expression of bone commitment markers including Collagen Type I, ALP, RUNX2, and osteocalcin in UC-MSCs cultured in the presence of exosome-enriched composite scaffold was 4 to 6 times higher than that of these markers in cells cultured with exosomes alone (Fig. 9). Indeed, the release of biologically active ions (calcium and phosphorus ions) from composite scaffold can affect the gene expression of UC-MSCs and activate their osteogenic commitment. This data is consistent with a study, where PLA-based scaffolds, in particular with the highest amount of mineral fillers (PLA-10CaSi-10DCPD), enriched with exosome enhanced the gene expression of human adipose tissue derived-MSCs.<sup>18</sup>

The study reported that the PAA/triCaPNPs scaffold in addition to offering good physicochemical and osteogenic properties due to the presence of CaPNPs, can also carry and release exosomes in a functional form into the medium. Our future study will focus on *in vivo* experiments. The bone regeneration effect of the exosome/composite scaffold will be assessed to achieve physical support of the defect and controlled exosome release in a bone defect animal model.

## Conclusion

The current research is the first study fabricating a 3D multiscale scaffold using triCaPNPs in the substrate of PPA polymer using a cross-linker and freeze-drying process. This study indicated that the presence of NPs in the PAA

substrate can improve the physicochemical properties of PAA polymer in favor of increasing bone differentiation. This scaffold could mimic the nanoscale structure and chemical combination of native bone minerals. So, our results suggest that the PAA/triCaPNPs scaffold could be beneficial to achieve controlled exosome release for exosome-based therapy in bone tissue engineering.

#### Acknowledgments

We thank the centers that sponsored this study.

#### Competing interests

There is no competing interest for authors.

#### Ethical Statement

Tarbiat Modares University's Medical Research Ethics Committee (IR.MODARES.REC.1398.093) and Shahid Beheshti University's Medical Research Ethics Committee (IR.SBMU.REC.1400.015) confirmed this study.

#### Funding

Tarbiat Modares University, Grant/Award Number: 9620792002; Council for Development of Stem Cell Sciences and Technologies, Grant/Award Number: 11/37701; Shahid Beheshti University of Medical Sciences: ID:26284.

#### References

- Henkel J, Woodruff MA, Epari DR, Steck R, Glatt V, Dickinson IC, et al. Bone Regeneration Based on Tissue Engineering Conceptions — A 21st Century Perspective. *Bone Res* **2013**; 1: 216-48. <https://doi.org/10.4248/BR201303002>
- Zhao Y, Li Z, Jiang Y, Liu H, Feng Y, Wang Z, et al. Bioinspired mineral hydrogels as nanocomposite scaffolds for the promotion of osteogenic marker expression and the induction of bone regeneration in osteoporosis. *Acta Biomaterialia* **2020**; 113: 614-26. <https://doi.org/10.1016/j.actbio.2020.06.024>
- Finkemeier CG. Bone-grafting and bone-graft substitutes. *J Bone Joint Surg Am* **2002**; 84: 454-64. <https://doi.org/10.2106/00004623-200203000-00020>
- Kim DH, Rhim R, Li L, Martha J, Swaim BH, Banco RJ, et al. Prospective study of iliac crest bone graft harvest site pain and morbidity. *Spine J* **2009**; 9: 886-92. <https://doi.org/10.1016/j.spinee.2009.05.006>
- Gomes KU, Carlini JL, Biron C, Rapoport A, Dedivitis RA. Use of allogeneic bone graft in maxillary reconstruction for installation of dental implants. *J Oral Maxillofac Surg* **2008**; 66: 2335-8. <https://doi.org/10.1016/j.joms.2008.06.006>
- Wiltfang J, Zernial O, Behrens E, Schlegel A, Warnke PH, Becker ST. Regenerative treatment of peri-implantitis bone defects with a combination of autologous bone and a demineralized xenogenic bone graft: a series of 36 defects. *Clin Implant Dent Relat Res* **2012**; 14: 421-7. <https://doi.org/10.1111/j.1708-8208.2009.00264.x>
- Djouad F, Bouffi C, Ghannam S, Noël D, Jorgensen C. Mesenchymal stem cells: innovative therapeutic tools for rheumatic diseases. *Nat Rev Rheumatol* **2009**; 5: 392-9. <https://doi.org/10.1038/nrrheum.2009.104>
- Bruno S, Collino F, Tetta C, Camussi G. Dissecting paracrine effectors for mesenchymal stem cells. *Adv Biochem Eng Biotechnol* **2013**; 129: 137-52. [https://doi.org/10.1007/10\\_2012\\_149](https://doi.org/10.1007/10_2012_149)
- Wang K-X, Xu L-L, Rui Y-F, Huang S, Lin S-E, Xiong J-H, et al. The effects of secretion factors from umbilical cord derived mesenchymal stem cells on osteogenic differentiation of mesenchymal stem cells. *PLoS one* **2015**; 10: e0120593-e. <https://doi.org/10.1371/journal.pone.0120593>
- Baglio SR, Pegtel DM, Baldini N. Mesenchymal stem cell secreted vesicles provide novel opportunities in (stem) cell-free therapy. *Front Physiol* **2012**; 3: 359. <https://doi.org/10.3389/fphys.2012.00359>
- Yang S, Zhu B, Yin P, Zhao L, Wang Y, Fu Z, et al. Integration of Human Umbilical Cord Mesenchymal Stem Cells-Derived Exosomes with Hydroxyapatite-Embedded Hyaluronic Acid-Alginate Hydrogel for Bone Regeneration. *ACS Biomater Sci Eng* **2020**; 6: 1590-602. <https://doi.org/10.1021/acsbomaterials.9b01363>
- Cheng H, Qiu L, Ma J, Zhang H, Cheng M, Li W, et al. Replicative senescence of human bone marrow and umbilical cord derived mesenchymal stem cells and their differentiation to adipocytes and osteoblasts. *Mol Biol Rep* **2011**; 38: 5161-8. <https://doi.org/10.1007/s11033-010-0665-2>
- Deuse T, Stubbendorff M, Tang-Quan K, Phillips N, Kay MA, Eiermann T, et al. Immunogenicity and immunomodulatory properties of umbilical cord lining mesenchymal stem cells. *Cell Transplant* **2011**; 20: 655-67. <https://doi.org/10.3727/096368910x536473>
- Hong B, Lee S, Shin N, Ko Y, Kim D, Lee J, et al. Bone regeneration with umbilical cord blood mesenchymal stem cells in femoral defects of ovariectomized rats. *Osteoporos Sarcopenia* **2018**; 4: 95-101. <https://doi.org/10.1016/j.afos.2018.08.003>
- Chen W, Liu X, Chen Q, Bao C, Zhao L, Zhu Z, et al. Angiogenic and osteogenic regeneration in rats via calcium phosphate scaffold and endothelial cell co-culture with human bone marrow mesenchymal stem cells (MSCs), human umbilical cord MSCs, human induced pluripotent stem cell-derived MSCs and human embryonic stem cell-derived MSCs. *J Tissue Eng Regen Med* **2018**; 12: 191-203. <https://doi.org/10.1002/term.2395>
- Chen W, Liu J, Manuchehrabadi N, Weir MD, Zhu Z, Xu HH. Umbilical cord and bone marrow mesenchymal stem cell seeding on macroporous calcium phosphate for bone regeneration in rat cranial defects. *Biomaterials* **2013**; 34: 9917-25. <https://doi.org/10.1016/j.biomaterials.2013.09.002>
- Zhang J, Liu X, Li H, Chen C, Hu B, Niu X, et al. Exosomes/tricalcium phosphate combination scaffolds can enhance bone regeneration by activating the PI3K/Akt signaling pathway. *Stem Cell Res Ther* **2016**; 7: 136. <https://doi.org/10.1186/s13287-016-0391-3>
- Gandolfi MG, Gardin C, Zamparini F, Ferroni L, Esposti MD, Parchi G, et al. Mineral-Doped Poly(L-lactide) Acid Scaffolds Enriched with Exosomes Improve Osteogenic Commitment of Human Adipose-Derived Mesenchymal Stem Cells. *Nanomaterials (Basel, Switzerland)* **2020**; 10: 432. <https://doi.org/10.3390/nano10030432>
- Lei Y, Gojgini S, Lam J, Segura T. The spreading, migration and proliferation of mouse mesenchymal stem cells cultured inside hyaluronic acid hydrogels. *Biomaterials* **2011**; 32: 39-47. <https://doi.org/10.1016/j.biomaterials.2010.08.103>
- Bai X, Lü S, Liu H, Cao Z, Ning P, Wang Z, et al. Polysaccharides based injectable hydrogel compositing bio-glass for cranial bone repair. *Carbohydr Polym* **2017**; 175: 557-64. <https://doi.org/10.1016/j.carbpol.2017.08.020>
- Argentiere S, Blasi L, Ciccarella G, Barbarella G, Cingolani R, Gigli G. Nanogels of poly(acrylic acid): Uptake and release behavior with fluorescent oligothiophene-labeled bovine serum albumin. *J Appl Polym Sci* **2010**; 116: 2808-15. <https://doi.org/10.1002/app.31691>
- Huang K, Wu J, Gu Z. Black Phosphorus Hydrogel Scaffolds Enhance Bone Regeneration via a Sustained Supply of Calcium-Free Phosphorus. *ACS Appl Mater Interfaces* **2019**; 11: 2908-16. <https://doi.org/10.1021/acsami.8b21179>
- Bheri S, Davis ME. Nanoparticle-Hydrogel System for Post-myocardial Infarction Delivery of MicroRNA. *ACS Nano* **2019**; 13: 9702-6. <https://doi.org/10.1021/acsnano.9b05716>
- Yuan W, Li Z, Xie X, Zhang Z-Y, Bian L. Bisphosphonate-based nanocomposite hydrogels for biomedical applications. *Bioact Mater* **2020**; 5: 819-31. <https://doi.org/10.1016/j.bioactmat.2020.06.002>
- Shi L, Wang F, Zhu W, Xu Z, Fuchs S, Hilborn J, et al. Self-Healing Silk Fibroin-Based Hydrogel for Bone Regeneration: Dynamic Metal-Ligand Self-Assembly Approach. *Advanced Functional Materials* **2017**; 27: 1700591. <https://doi.org/10.1002/adfm.201700591>

26. Kadajji VG, Betageri GV. Water Soluble Polymers for Pharmaceutical Applications. *Polymers* **2011**; 3: 1972-2009.
27. Swift T, Swanson L, Geoghegan M, Rimmer S. The pH-responsive behaviour of poly(acrylic acid) in aqueous solution is dependent on molar mass. *Soft Matter* **2016**; 12: 2542-9. <https://doi.org/10.1039/C5SM02693H>
28. des Rieux A, Fievez V, Garinot M, Schneider YJ, Pr at V. Nanoparticles as potential oral delivery systems of proteins and vaccines: a mechanistic approach. *J Control Release* **2006**; 116: 1-27. <https://doi.org/10.1016/j.jconrel.2006.08.013>
29. Pourbasher S, Shahrsvand M, Ghaffari M. Preparation and characterization of semi-IPNs of polycaprolactone/poly (acrylic acid)/cellulosic nanowhisker as artificial articular cartilage. *Int J Biol Macromol* **2020**; 142: 298-310.
30. Zhang Y, Wu H, Yuan B, Zhu X, Zhang K, Zhang X. Enhanced osteogenic activity and antibacterial performance in vitro of polyetheretherketone by plasma-induced graft polymerization of acrylic acid and incorporation of zinc ions. *J Mater Chem B* **2021**; 9: 7506-7515. <https://doi.org/10.1039/d1tb01349a>
31. Ayers D, Cuthbertson JM, Schroyer K, Sullivan SM. Polyacrylic acid mediated ocular delivery of ribozymes. *J Control Release* **1996**; 38: 167-75.
32. Hajikhani M, Khangahi MM, Shahrsvand M, Mohammadi-Rovshandeh J, Babaei A, Khademi SMH. Intelligent superabsorbents based on a xanthan gum/poly (acrylic acid) semi-interpenetrating polymer network for application in drug delivery systems. *Int J Biol Macromol* **2019**; 139: 509-20.
33. Qiu Y, Park K. Environment-sensitive hydrogels for drug delivery. *Adv Drug Deliv Rev* **2001**; 53: 321-39. [https://doi.org/10.1016/s0169-409x\(01\)00203-4](https://doi.org/10.1016/s0169-409x(01)00203-4)
34. Wang X, Zhang M, Zhang L, Li L, Li S, Wang C, et al. Designed Synthesis of Lipid-Coated Polyacrylic Acid/Calcium Phosphate Nanoparticles as Dual pH-Responsive Drug-Delivery Vehicles for Cancer Chemotherapy. *Chemistry* **2017**; 23: 6586-95. <https://doi.org/10.1002/chem.201700060>
35. Li L, Zhang L, Wang T, Wu X, Ren H, Wang C, et al. Facile and Scalable Synthesis of Novel Spherical Au Nanocluster Assemblies@ Polyacrylic Acid/Calcium Phosphate Nanoparticles for Dual-Modal Imaging-Guided Cancer Chemotherapy. *Small* **2015**; 11: 3162-73. <https://doi.org/10.1002/sml.201403517>
36. Lee JS, Murphy WL. Functionalizing calcium phosphate biomaterials with antibacterial silver particles. *Adv Mater* **2013**; 25: 1173-9. <https://doi.org/10.1002/adma.201203370>
37. Li X, Wang X, Sogo Y, Ohno T, Onuma K, Ito A. Mesoporous silica-calcium phosphate-tuberculin purified protein derivative composites as an effective adjuvant for cancer immunotherapy. *Adv Healthc Mater* **2013**; 2: 863-71. <https://doi.org/10.1002/adhm.201200149>
38. Maitra A. Calcium phosphate nanoparticles: second-generation nonviral vectors in gene therapy. *Expert Rev Mol Diagn* **2005**; 5: 893-905. <https://doi.org/10.1586/14737159.5.6.893>
39. Barroug A, Kuhn L, Gerstenfeld L, Glimcher M. Interactions of cisplatin with calcium phosphate nanoparticles: in vitro controlled adsorption and release. *Journal of Orthopaedic Research* **2004**; 22: 703-8.
40. LeGeros RZ. Calcium phosphate-based osteoinductive materials. *Chem Rev* **2008**; 108: 4742-53. <https://doi.org/10.1021/cr800427g>
41. Bose S, Tarafder S. Calcium phosphate ceramic systems in growth factor and drug delivery for bone tissue engineering: A review. *Acta Biomaterialia* **2012**; 8: 1401-21. <https://doi.org/10.1016/j.actbio.2011.11.017>
42. Hosseinzadeh S, Soleimani M, Vashegani Farahani E, Ghanbari H, Arkan E, Rezaayat SM. Detailed mechanism of aniline nucleation into more conductive nanofibers. *Synthetic Metals* **2015**; 209: 91-8. <https://doi.org/10.1016/j.synthmet.2015.06.005>
43. LeGeros RZ. Properties of osteoconductive biomaterials: calcium phosphates. *Clin Orthop Relat Res* **2002**; 81-98. <https://doi.org/10.1097/00003086-200202000-00009>
44. Blom EJ, Klein-Nulend J, Wolke JG, van Waas MA, Driessens FC, Burger EH. Transforming growth factor-beta1 incorporation in a calcium phosphate bone cement: material properties and release characteristics. *J Biomed Mater Res* **2002**; 59: 265-72. <https://doi.org/10.1002/jbm.1241>
45. Weir MD, Xu HHK. High-strength, in situ-setting calcium phosphate composite with protein release. *J Biomed Mater Res A* **2008**; 85: 388-96. <https://doi.org/10.1002/jbm.a.31347>
46. Khoramgah MS, Ranjbari J, Abbaszadeh H-A, Tabatabaei Mirakabad FS, Hatami S, Hosseinzadeh S, et al. Freeze-dried multiscale porous nanofibrous three dimensional scaffolds for bone regenerations. *BioImpacts* **2020**; 10: 73-85. <https://doi.org/10.34172/bi.2020.10>
47. Gupta NV, Shivakumar HG. Investigation of Swelling Behavior and Mechanical Properties of a pH-Sensitive Superporous Hydrogel Composite. *Iran J Pharm Res* **2012**; 11: 481-93. <https://doi.org/10.22037/ijpr.2012.1097>
48. Embree MC, Chen M, Pylawka S, Kong D, Iwaoka GM, Kalajzic I, et al. Exploiting endogenous fibrocartilage stem cells to regenerate cartilage and repair joint injury. *Nat Commun* **2016**; 7: 13073-. <https://doi.org/10.1038/ncomms13073>
49. Th ery C, Amigorena S, Raposo G, Clayton A. Isolation and characterization of exosomes from cell culture supernatants and biological fluids. *Curr Protoc Cell Biol* **2006**; Chapter 3:Unit 3.22. <https://doi.org/10.1002/0471143030.cb0322s30>
50. Kolk A, Handschel J, Drescher W, Rothamel D, Kloss F, Blessmann M, et al. Current trends and future perspectives of bone substitute materials - from space holders to innovative biomaterials. *J Craniomaxillofac Surg* **2012**; 40: 706-18. <https://doi.org/10.1016/j.jcms.2012.01.002>
51. Herth G, Schornick G, L. Buchholz F. Polyacrylamides and Poly(Acrylic Acids). *Ullmann's Encyclopedia of Industrial Chemistry*. p. 1-16.
52. Lin K, Xia L, Gan J, Zhang Z, Chen H, Jiang X, et al. Tailoring the nanostructured surfaces of hydroxyapatite bioceramics to promote protein adsorption, osteoblast growth, and osteogenic differentiation. *ACS Appl Mater Interfaces* **2013**; 5: 8008-17. <https://doi.org/10.1021/am402089w>
53. Jafarigol E, Salehi MB, Mortaheb HR. Preparation and assessment of electro-conductive poly(acrylamide-co-acrylic acid) carboxymethyl cellulose/reduced graphene oxide hydrogel with high viscoelasticity. *Chem Eng Res Des* **2020**; 162: 74-84. <https://doi.org/10.1016/j.cherd.2020.07.020>
54. Li Q, Gong J, Zhang J. Rheological Properties and Microstructures of Hydroxyethyl Cellulose/Poly(Acrylic Acid) Blend Hydrogels. *Journal of Macromolecular Science, Part B* **2015**; 54: 1132-43. <https://doi.org/10.1080/00222348.2015.1077300>
55. Li N, Cui W, Cong P, Tang J, Guan Y, Huang C, et al. Biomimetic inorganic-organic hybrid nanoparticles from magnesium-substituted amorphous calcium phosphate clusters and polyacrylic acid molecules. *Bioactive Materials* **2021**; 6: 2303-14. <https://doi.org/10.1016/j.bioactmat.2021.01.005>
56. Kabiri K, Omidian H, Hashemi SA, Zohuriaan-Mehr MJ. Synthesis of fast-swelling superabsorbent hydrogels: effect of crosslinker type and concentration on porosity and absorption rate. *European Polymer Journal* **2003**; 39: 1341-8. [https://doi.org/10.1016/S0014-3057\(02\)00391-9](https://doi.org/10.1016/S0014-3057(02)00391-9)
57. Yi H, Ur Rehman F, Zhao C, Liu B, He N. Recent advances in nano scaffolds for bone repair. *Bone Res* **2016**; 4: 16050-. <https://doi.org/10.1038/boneres.2016.50>
58. Vlacic-Zischke J, Hamlet SM, Friis T, Tonetti MS, Ivanovski S. The influence of surface microroughness and hydrophilicity of titanium on the up-regulation of TGF /BMP signalling in osteoblasts. *Biomaterials* **2011**; 32: 665-71. <https://doi.org/10.1016/j.biomaterials.2010.09.025>
59. Chan O, Coathup MJ, Nesbitt A, Ho CY, Hing KA, Buckland T, et al. The effects of microporosity on osteoinduction of calcium phosphate bone graft substitute biomaterials. *Acta Biomater* **2012**; 8: 2788-94. <https://doi.org/10.1016/j.actbio.2012.03.038>
60. Ahmed EM. Hydrogel: Preparation, characterization, and

- applications: A review. *Journal of Advanced Research* **2015**; 6: 105-21. <https://doi.org/10.1016/j.jare.2013.07.006>
61. Ghaffari-Bohlouli P, Zahedi P, Shahrousvand M. Enhanced osteogenesis using poly (l-lactide-co-d, l-lactide)/poly (acrylic acid) nanofibrous scaffolds in presence of dexamethasone-loaded molecularly imprinted polymer nanoparticles. *Int J Biol Macromol* **2020**; 165: 2363-77. <https://doi.org/10.1016/j.ijbiomac.2020.10.078>
  62. Hosseini SM, Shahrousvand M, Shojaei S, Khonakdar HA, Asefnejad A, Goodarzi V. Preparation of superabsorbent eco-friendly semi-interpenetrating network based on cross-linked poly acrylic acid/xanthan gum/graphene oxide (PAA/XG/GO): Characterization and dye removal ability. *Int J Biol Macromol* **2020**; 152: 884-93. <https://doi.org/10.1016/j.ijbiomac.2020.02.082>
  63. Rivero RE, Capella V, Cecilia Liaudat A, Bosch P, Barbero CA, Rodríguez N, et al. Mechanical and physicochemical behavior of a 3D hydrogel scaffold during cell growth and proliferation. *RSC Adv* **2020**; 10: 5827-37. <https://doi.org/10.1039/c9ra08162c>
  64. Hosseinzadeh S, Rezayat SM, Vashgani-Farahani E, Mahmoudifard M, Zamanlui S, Soleimani M. Nanofibrous hydrogel with stable electrical conductivity for biological applications. *Polymer* **2016**; 97: 205-16.
  65. Jeong J, Kim JH, Shim JH, Hwang NS, Heo CY. Bioactive calcium phosphate materials and applications in bone regeneration. *Biomater Res* **2019**; 23: 1-11.
  66. Jia Y, Qiu S, Xu J, Kang Q, Chai Y. Exosomes Secreted by Young Mesenchymal Stem Cells Promote New Bone Formation During Distraction Osteogenesis in Older Rats. *Calcified Tissue International* **2020**; 106: 509-17. <https://doi.org/10.1007/s00223-019-00656-4>
  67. Zhu Y, Jia Y, Wang Y, Xu J, Chai Y. Impaired Bone Regenerative Effect of Exosomes Derived from Bone Marrow Mesenchymal Stem Cells in Type 1 Diabetes. *Stem Cells Transl Med* **2019**; 8: 593-605. <https://doi.org/10.1002/sctm.18-0199>
  68. Li W, Liu Y, Zhang P, Tang Y, Zhou M, Jiang W, et al. Tissue-Engineered Bone Immobilized with Human Adipose Stem Cells-Derived Exosomes Promotes Bone Regeneration. *ACS Appl Mater Interfaces* **2018**; 10: 5240-54. <https://doi.org/10.1021/acsami.7b17620>